 https://doi.org/10.3311/PPch.20589

Periodica Polytechnica Chemical Engineering, 67(1), pp. 94–103, 2023

Processing and Characterization of Polypropylene Nanocomposite Films Reinforced with Hexagonal Boron Nitride Nanosheets

Gülay Bayramoğlu[1*], Mehmet Mudu[2]

[1] Yalova Vocational School, Department of Textile - Clothing, Shoes and Leather, Yalova University, 87 Mehmet Durmam Caddesi , 77100 Yalova Turkey
[2] Institute of Graduate Studies, Department Polymer Materials Engineering, Yalova University, 77200 Yalova, P.O.B. 77100, Turkey
* Corresponding author, e-mail: gulayb@yalova.edu.tr

Received: 02 June 2022, Accepted: 13 September 2022, Published online: 09 January 2023

Abstract

In this study, we synthesized hexagonal boron nitride nanosheets (h-BNN) via the molten hydroxide exfoliation method which results in small flakes and nanoscrolls. The resultant h-BNNs can be dispersed in various solvents such as water, ethanol, and acetone, and form a stable dispersion. The morphological and structural analysis of h-BNNs were performed with Fourier Transform infrared spectroscopy (FTIR), X-ray diffractometry (XRD), and scanning electron microscopy (SEM). The masterbatch (MB) method was used to incorporate the h-BNNs into the polypropylene (PP) matrix via melt mixing. Dilution and film production processes were performed using a twin screw extruder. Nanocomposite films having an h-BNN weight ratio of 1%, 2%, 3%, and 5% were prepared. Thermogravimetric analyzer (TGA) and differential scanning calorimetry (DSC) were used to investigate the thermal stability. Crystallization (T_c) temperatures were increased with the increased amount of h-BNNs and h-BNNs nucleating agent behavior on the ***PP*** crystallization was observed. Oxidation induction time (OIT) of the pure PP was increased from 8.84 min to 17.82 min. The results show a considerable effect of the h-BNN content on the thermo-oxidative stability of the nanocomposites studied. The rheological and mechanical properties of the PP-hBNN nanocomposite films were also determined depending on the particle loading ratio. Optimum particle content providing the best thermal, mechanical, and rheological properties were found to be 3% wt.

Keywords

nanocomposite films, hexagonal boron nitride nanosheets, polypropylene, oxidation induction time

1 Introduction

Due to their superior properties against other materials, polymer nanocomposites (PNC) have been intensively studied, particularly in the last decades. PNCs are tailored to be superior properties that are specialized but also very effective. They consolidate different properties of traditional materials and perform a wide range of functions and purposes which cannot be achieved by them. Their ascendant thermal, mechanical, chemical and tribological properties widen its usability potential in different applications such as automobile components, advanced medical applications, drug delivery systems, multifunctional materials, microelectronic packaging coatings, and flame retardants [1–6]. One can suggest from their name that PNCs are the combination of a nanoscale reinforcement and polymer matrix and they possess the most desirable properties of the reinforcement and polymer matrix. Nano clay, nano oxides, graphene, metallic nanoparticles such as nano titanium or nano copper, and carbon nanotubes (CNT) are the most common reinforcements used in the preparation of PNCs [7, 8]. PNCs also provide design and process flexibility due to the almost limitless number of reinforcement and polymer matrix combinations. On the other hand, there are also numerous challenges that limit the performance of PNCs such as reinforcement dispersion, particle-chain interactions, interfaces, and interphase strengths [9, 10]. To overcome these challenges researchers have been performing different strategies such as surface modification of reinforcement, utilizing surfactant, or using co-matrix/particles [11–13]. Boron nitrides (BN) are one of the most preferred fillers which consist of boron-nitrogen bonds. The most known crystalline forms of BN are cubic form (c-BN) which is isoelectronic with diamond; wurtzite BN (w-BN) and hexagonal boron nitride (hBN) which is isoelectronic with graphite [14]. Unlike hBN, wBN and cBN are stable at high pressures and temperatures. hBN is stable

Cite this article as: Bayramoğlu, G., Mudu, M. "Processing and Characterization of Polypropylene Nanocomposite Films Reinforced with Hexagonal Boron Nitride Nanosheets", Periodica Polytechnica Chemical Engineering, 67(1), pp. 94–103, 2023. https://doi.org/10.3311/PPch.20589

at room temperature and it is a white, non-toxic, and impermeable material with almost the lowest density (2.27 g/cm^3) among ceramic materials [15]. The 2-D nanosheets of hBN (h-BNNs) are known as white graphene and are beneficial for PNCs. Besides the improved optical properties and chemical stability; with their high surface area, they reduce interchain mobility and improve the mechanical and thermal properties of polymers. Due to their fascinating properties, they have great potential in various applications including coatings, automotive, catalysts, medicine, sensors, electronics, high-resolution imaging, energy storage, water purification, and UV emitters [16–19]. The h-BNNs can be prepared by using various methods. Chemical exfoliation, ball milling, mechanical cleavage, molten exfoliation, chemical vapor deposition, high energy radiation, and biomass-directed synthesis have been reported for the fabrication of h-BNNs [20–24].

In this study, hexagonal boron nitride nanosheets (h-BNN) were prepared via molten hydroxide exfoliation, and a range of h-BNN/polypropylene nanocomposite films was prepared. Since the h-BNN nanosheets tend to stack to each other, melt-mixing and extrusion methods were used to prepare films to eliminate further aggregation. The detailed investigations on the preparation and morphology of both h-BNNs and h-BNN/polypropylene nanocomposites were carried out via field emission scanning electron microscope equipped with a transmission electron detector (STEM) and X-ray diffraction (XRD) analysis. The effects of h-BNN content on the rheological, processing, thermal and mechanical properties of nanocomposites were also investigated.

2 Materials and methods

2.1 Materials

Hexagonal boron nitride (≥99.9%, Ma: 24.8 g/mol, white powder) was supplied from BORTEK, Boron Technologies, and Mechatronics Inc., Turkey. Sodium hydroxide (NaOH) (reagent grade, ≥98%, pellets) and potassium hydroxide (KOH) (reagent grade, 90%, flakes) were purchased from Sigma-Aldrich. Polypropylene (PP) (Y101) (MFI of 15 g / 10 min (230 °C, 2.16 kg) and density of 0.9 g/cm^3 was supplied from the Sumitomo Corporation.

2.2 Methods

2.2.1 Exfoliation of hBN

The exfoliation procedure was carried out as described elsewhere [24]. After mixing 0.05 mol (2.0 g) sodium hydroxide (NaOH) and 0.05 mol (2.8055 g) potassium hydroxide (KOH), the agate was pulverized using a mortar. 0.01 mol (0.284 g) of h-BN was added to the mixture and stirring was continued. After obtaining a homogeneous mixture, the mixture was transferred to the poly(tetrafluoroethylene) – lined stainless steel hydrothermal synthesis reactor. The reactor was kept at 180 °C for 2 hours in an oven. After 2 hours, the temperature was turned off and the oven was cooled down to room temperature without opening the lid. The solid in the reactor was washed with ethanol and deionized water until the filtrate was neutral and dried under vacuum for 12 hours. Exfoliated hBN nanosheets (h-BNNs) were observed by scanning electron microscopy (SEM); used for nanocomposite preparation and characterization.

2.2.2 Preparation of the h-BNN / polypropylene nanocomposites

Since the nanofiller content is too low; the masterbatch (MB) method was used to prepare the base compound. The PP and h-BNNs were dried in an oven at 80 °C for approximately 10 h until they reached 1% moisture content. PP and h-BNNs were mixed by thermal compounding using a melt mixer to obtain an MB containing 20% h-BNN. The mixing process was carried out within 5 minutes at 190 °C with a rotor speed of 80 rpm.

The melt was solidified directly by air-cooling and pelletized using a laboratory scale pelletizer (Gülnar Machine, Turkey).

2.2.3 Nanocomposite film production

In this step, the masterbatch (MB) was diluted to various amounts of hBNN (1%, 2%, 3%, and 5% wt) content. Both the dilutionand film production were performed using a twin screw extruder. The extruder was a co-rotating intermeshing extruder (Gülnar Machine, Turkey) with a 16 mm screw diameter and a 24:1 length-to-diameter ratio (L/D). The extruder was also equipped with a cast film unit. During the extrusion barrel temperatures of the five zones were set as 140 °C, 160 °C, 200 °C, 210 °C, and 220 °C from feeding to die zones and the screw speed was maintained at 250 rpm.

2.3 Characterization tests

Fourier Transform Infrared (FT-IR) spectrum was recorded on Bruker Alpha ATR-FTIR spectrophotometer in the range of 4000–650 cm^{-1} at room temperature with the 4 cm^{-1} resolution mode.

XRD analysis of the hBN and hBNN particles were recorded on Rigaku D/Max-Ultimate X-Ray diffractometer with CuK_α radiation (λ = 1.5406 Å), operating at 40 kV and 40 mA and a rate of 0.2°/min.

The crystal structure examinations (interlayer distances (d) crystallite thicknesses (L_c), lateral size (L_a), full-width at half maximum (FWHM)) of h-BNNs were also confirmed via powder XRD measurements. The interlayer distance was estimated from the 002 reflection (peak at 26.72°) by applying Bragg's law. Both crystallite thicknesses (L_c) and lateral size (L_a) were calculated from the 002 (peak at 26.72°) and 100 reflections (peak at 41.61°) according to Scherrer's equation Eq. (1) The number of layers was also calculated by the ratio L_c/d.

$$L = \frac{K\lambda}{\beta \cos\theta} \tag{1}$$

Here L is the average grain size (L_c or L_a of the h-BNNs, K is the dimensionless shape factor (K = 0.94 and K = 1.84 used for L_c and L_a, respectively), λ is the wavelength (0.15406 nm) of the X-ray, β is the line broadening at half the maximum intensity and θ is the Bragg angle [25].

Thermogravimetric analysis (TGA) of the PP-hBNN nanocomposite films was carried out on a Seiko SII TG/DTA 7300 Thermogravimetric analyzer. Samples were heated from 25 to 700 °C with a heating rate of 10 °C/min in nitrogen.

Thermal transitions of the nanocomposite films were characterized by a differential scanning calorimeter (Pyris Diamond DSC) under nitrogen atmosphere. In the first run, the nanocomposites were heated from 25 °C to 200 °C with a heating rate of 10 °C/min and isothermally kept at that temperature for 1 min. To observe crystallization transition, we performed the second run where the materials were cooled to 35 °C at a heating rate of 10 °C/min. In the last run, samples were heated to 200 °C with a heating rate of 10 °C/min. The endothermic peaks observed in the third run of the DSC studies were used to determine the melting transitions.

Oxidation induction time measurements were carried out using Pyris Diamond DSC under the conditions stated in ASTM D-3895-07. Approximately 10 mg sample was placed in an uncovered pan and subjected to nitrogen gas. The DSC cell is heated to the temperature of 200 °C (heating rate of 10 °C min^{-1}) where the OIT value was determined. After reaching 200 °C samples were held about 3 min for under isothermal conditions where the phase was indicated as t^1 and then nitrogen was switched to oxygen gas. The flow of both gases was adjusted to 50 mL min^{-1} during the entire measurement. The DSC cell was held under isothermal conditions until a significant exothermic onset (oxidation) was obtained. The onset of this oxidation signal was indicated as t^2. The difference between t^1 and t^2 was calculated as OIT time.

To evaluate the hBNN-PP interactions and morphology of the PP-hBNN nanocomposite films were observed by Philips XL30 ESEM-FEG/EDAX Scanning electron microscope (SEM). Prior to the sample observation, film samples were broken in liquid nitrogen and the fractured surfaces were covered with a platinum layer with an Edwards S 150 B sputter coater. hBNNs were also investigated by JEOL JSM-7600F (Field Emission Scanning Electron Microscope) equipped with a TED (Transmission Electron Detector). For this purpose, 200 mesh, Holey Carbon Grid was used. An ultrasonic bath was used to disperse the hBNNs in isopropyl alcohol. After 15 min sonication, the solution was dropped on the copper TEM grid and dried.

Zwick Roell Z010/TN2S Materials Testing Machine in tensile mode at room temperature with a load cell of 20kN using a crosshead speed of 500 mm/min. The nanocomposite films were obtained using a cutting device in accordance with ISO 527-3 standard [26]. Mechanical tests were repeated at least 5 times for each sample and mean values were taken.

The rheological properties of the PP-hBNN nanocomposite films were carried out with a rotational dynamic oscillatory rheometer (Discovery Hybrid Rheometer-1, DHR-1, TA Instruments) equipped with a parallel plate that was 25 mm in diameter. Measurements were performed with a gap distance of 1000μm at 200 °C.

3 Results and discussion

3.1 Preparation of h-BNNs

h-BNNs were synthesized by the molten hydroxide exfoliation method. The exfoliation process depends on the insertion of cations (Na^+ or K^+) and anions (OH^-) between h-BN layers. Due to their chemical potentials, they insert into interlayer space on the top surface. Using NaOH as only hydroxide was found to be not enough for exfoliation [24]. Because of that solid mixed NaOH/KOH with a molar ratio of 1:1 was found to be the optimum condition for the exfoliation process.

Since the exfoliation media is highly alkaline, KOH or NaOH residues can affect some properties of nanocomposite film. Removal of hydroxides and exfoliation process of the bulk h-BN particles as well as chemical properties of h-BNNs were investigated by ATR-IR analysis.

The ATR-IR spectra of the h-BN and h-BNNs are shown in Fig. 1. In the ATR-IR spectra, two strong characteristic peaks were detected around 1380 cm^{-1} and 770 cm^{-1} which belong to in-plane B-N stretching vibration and out-of-plane B-N-B bending vibration, respectively.

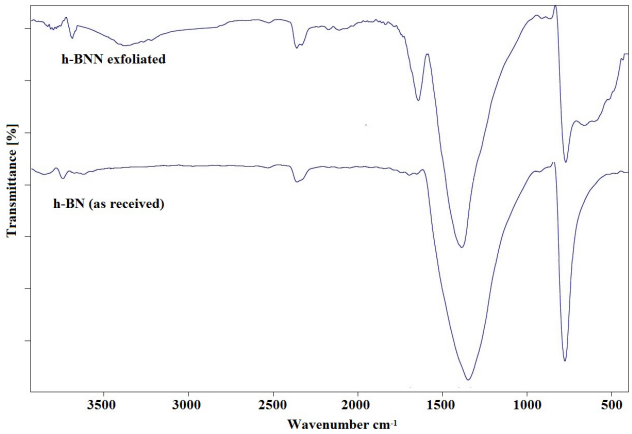

Fig. 1 ATR-IR spectra of as received and exfoliated h-BN nanosheets

Besides, a weak and broad band at about 3340 cm^{-1} is attributed to hydroxyl group formation on the h-BNN layers which was also confirmed by XRD analysis.

The exfoliation process of the bulk h-BN particles was confirmed via XRD analysis. The XRD diffraction patterns of bulk h-BN and h-BNNs are given in Fig. 2. As seen in Fig. 2, the diffraction peaks which are located at 2θ = 26.8°, 41.6°, 43.9°, 50.2° and 55.2°, are correspond to crystal planes of (002), (100), (101), (102) and (004) respectively, are accordance with JCPDS (Joint Committee on Powder Diffraction Standards – Card no. 34-0421) for standard h-BN powders [27]. In addition to the peaks reported for h-BN in JCPDS, the presence of a new peak observed at 2θ = 30.0° attributed to the (010) plane. This new peak indicates that h-BN layers are exfoliated to form nanosheets and -OH groups are exposed on their surfaces due to the harsh alkaline exfoliation method.

The crystallite thickness and crystallite lateral size of the h-BNNs were found to be 3.96 and 11.29 nm, respectively. The number of layers was also calculated as 11.9.

The morphology of h-BN and h-BNNs were evaluated by SEM and STEM analyses. SEM analyses were first performed on bulk h-BN (as-obtained h-BN) and h-BNN. It can be seen in Fig. 3(a) that bulk h-BN powders consist of irregular shapes and thick flakes which are stacked on each other with different lateral sizes.

STEM images in Fig. 3(c) and (d) reveal that the exfoliation process of bulk h-BN is sufficient since the thickness and lateral sizes of the exfoliated particles decreased and a single to a few layered h-BNNs formed. High magnification STEM images in Fig. 3(c) also show that some of

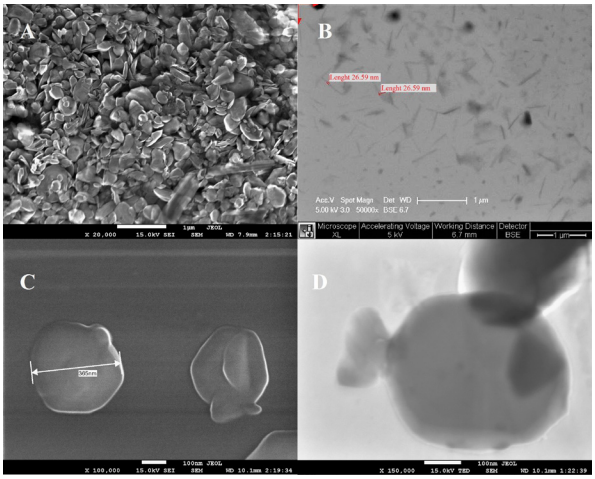

Fig. 3 SEM an STEM images of (a) SEM image of bulk h-BN particles, (b) STEM image h-BNN scrolls, (c) STEM images of the exfoliated h-BNNs; (d) SEM images of exfoliated h-BNN's at x150000 magnification

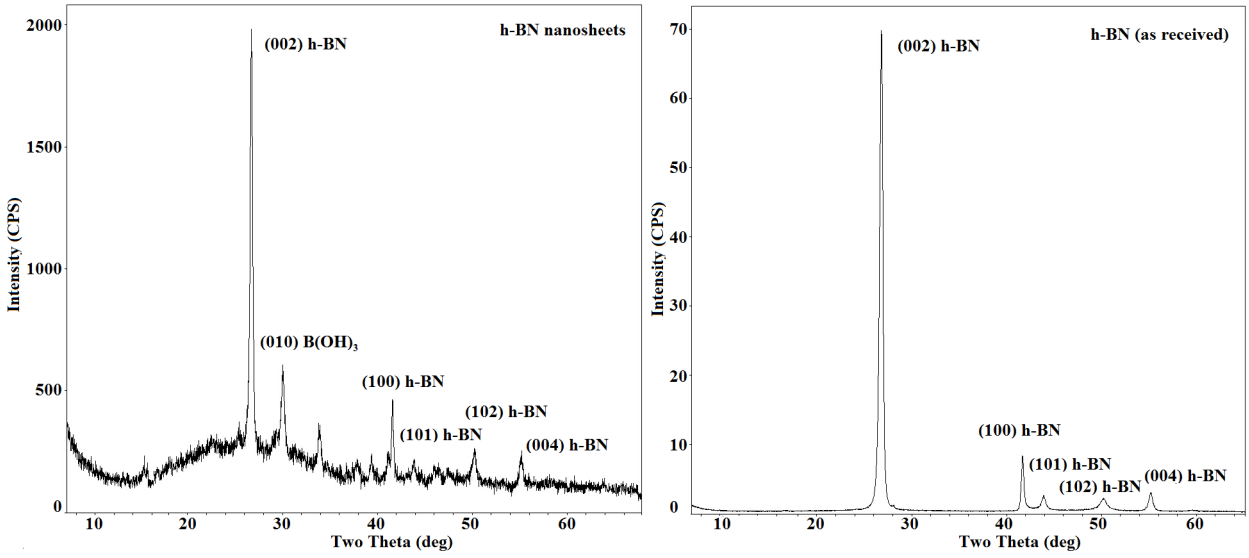

Fig. 2 XRD diffraction patterns of bulk h-BN and exfoliated h-BN nanosheets

the single-layered h-BNNs are partially rolled into a roll by curling at one end. One can see from Fig. 3(d) entirely transparent nanosheets that show their ultrathin nature, unlike bulk h-BN particles. The size of the h-BNN scrolls ranges from 27 nm to 217 nm while h-BNNs range from 200 nm to 500 nm.

3.2 *PP* nanocomposites

3.2.1 Thermal properties

The TGA and the differential thermogravimetric (DTG) curves of PP-h-BNN nanocomposite films with various contents of h-BNNs powders are presented in Fig. 4. 10% weight loss temperature (Td_{10}), 50% weight loss temperature (Td_{50}), the maximum decomposition rate MDRmax and char % at 700 °C are summarized in Table 1.

One can see from Table 1 that, Td_{10} and Td_{50} temperatures were slightly increased with the increasing h-BNN content.

On the other hand, MDR_{max} of the nanocomposites was decreased up to a critical h-BNN content which is 3 wt%. When the h-BNN content increase to 5 wt%. The MDR_{max} decreases about 10% compared to the neat PP matrix. This phenomenon can be attributed to the stacking of h-BNN particles.

TGA curves in Fig. 4 show that neat PP and all nanocomposites exhibit identical degradation properties, with a single-step decomposition, revealing that h-BNN content has no significant effect on the thermal degradation mechanism. Aside from the mechanism, TGA analysis proves that h-BNN improves the thermal stability of nanocomposites. This may be due to the high thermal conductivity of h-BNNs and the strong interaction with the PP matrix.

The DSC method is one of the most common methods to investigate the numerous phenomena of nanocomposites such as melting, crystallization, and glass transition (T_g).

The heat characteristics of the prepared PP-h-BNN nanocomposite films were examined using DSC.

The DSC thermograms of neat PP and nanocomposites were shown in Fig. 5 while the crystallization temperature (T_c) and melting temperature (T_m) were collected in Table 2. Neat PP and PP-h- BNN nanocomposite showed single melting peaks during the heating. As can be seen from Fig. 5, the crystallization temperature (T_c) of the PP matrix was remarkably shifted to the higher temperatures. It can be said that semi-crystalline h-BNNs behave as a nucleating agent of PP crystallization. According to Fig. 5, the addition of the h-BNN particles slightly changed the melting temperature (T_m) of the PP-h-BNN nanocomposites. The degree of crystallinity (X_c) of the nanocomposites was calculated with the following Eq. (2)

Table 1 TGA analysis of the neat PP and PP-h-BNN nanocomposite films

Sample	Td_{10} (°C)	Td_{50} (°C)	Max. decomposition rate (μg/min, °C)	Char at 700 °C (%)
PP	425	452	1942	5.42
PP-hBNN-1	427	454	1431	6.31
PP-hBNN-2	436	457	1182	7.27
PP-hBNN-3	436	458	1078	7.61
PP-hBNN-5	435	459	1763	8.25

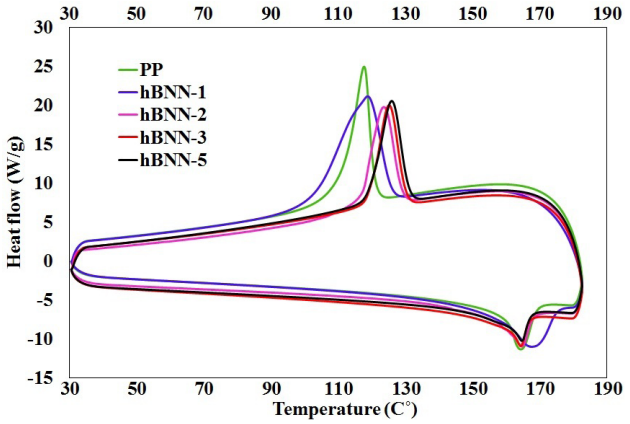

Fig. 5 The DSC thermograms of the neat PP and PP-h-BNN nanocomposite films

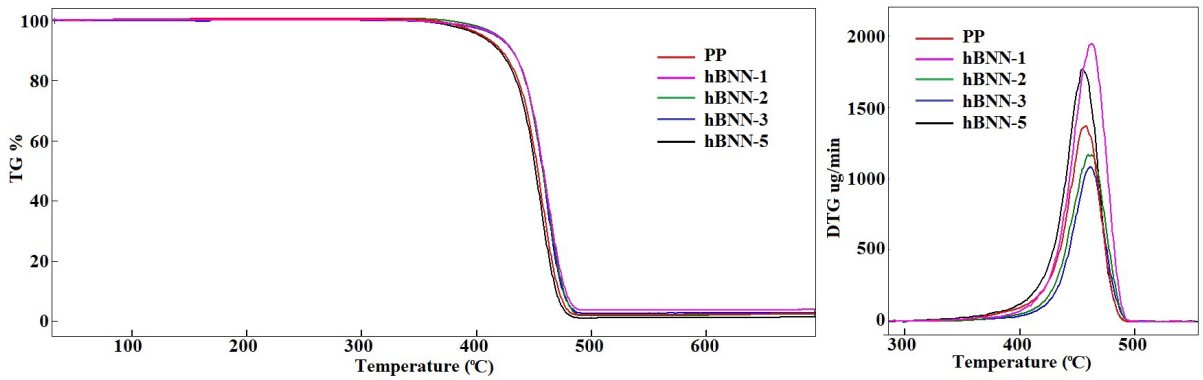

Fig. 4 TGA and DTA curves of neat PP and PP-h-BNN nanocomposite films

Table 2 The specific melting enthalpy (ΔH_m), melting temperature (T_m), the degree of crystallinity (X_c) and the crystallinity temperature (T_c) of the neat PP and PP-h-BNN nanocomposite films

Sample	T_m (°C)	ΔH_m (J/g)	T_c (°C)	ΔH_c (J/g)	X_c (%)
PP	166.9	77.1	117.8	-84.0	32.2
PP-hBNN-1	169.0	61.2	118.9	-61.3	29.7
PP-hBNN-2	166.8	52.4	125.2	-61.7	26.6
PP-hBNN-3	165.6	54.2	126.2	-59.8	26.9
PP-hBNN-5	166.0	68.5	126.8	-59.3	36.2

$$X_c = \frac{\delta H_m}{(1-f)\delta H_0}, \quad (2)$$

where ΔH_m is the melting enthalpy, f is the mass fraction of the PP matrix and ΔH_0 is the melting enthalpy of the 100% crystalline PP, which was reported to be 208 J g^{-1} [28]. Consistent with the previous studies, with the increase of the h-BNN content, the degree of crystallinity of the PP-h-BNN nanocomposites decreases [29, 30].

The stacking of h-BNN particles at higher loadings changes the particle size and blocks the crystallization of the PP matrix. The small size of h-BNNS contributes to the rapid energy release which also reduces the crystallization of the PP matrix.

DSC was also used to explore the oxidation induction time (OIT) and the OIT is evaluated in accordance with Fig. 6. Oxidative induction time gives information about the thermo-oxidative performance of the sample and the higher oxidation resistance provides the high OIT value [31]. The samples were heated up to 200 °C under nitrogen gas, and then oxygen gas was loaded into the system.

The time until the start of the exothermic process was measured. As can be seen from Fig. 6 that h-BNN addition significantly increases the required time for oxidation of the nanocomposites in comparison to neat polypropylene which indicates that the fire resistance increases. This phenomenon can be attributed to the higher thermal stability and good resistance to oxidation of h-BNNs.

3.2.2 Mechanical properties

The thicknesses of the prepared test samples were measured with calipers and averaged. The films were attached between the jaws of the tensile device from the ends and the distance between the two jaws was precisely adjusted. The separation speed of the jaws was set at 500 mm/min. The tensile test was continued until the moment of rupture. Mechanical tests were repeated 5 times for each sample. The stress-strain experiments in the tensile device were performed according to the ISO method and at room temperature. Elongation % and ultimate force values were found by using the tensile strength values corresponding to the elongation. The results of the experiment for all specimens studied are given in Table 3 and Fig. 7.

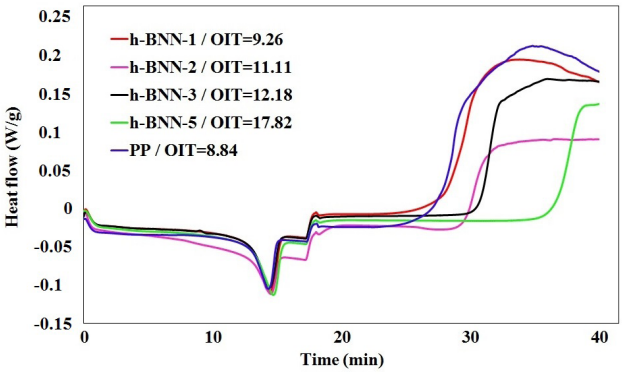

Fig. 6 Oxidation induction time (OIT) curves of the neat ***PP*** and PP-h-BNN nanocomposite films

Table 3 The tensile test results of the neat PP and PP-h-BNN nanocomposite films

Sample	Tensile strength (Mpa)	Yield strength (Mpa)	Elongation at break (%)	Elastic modulus (Mpa)
PP	25.86	34.86	362.58	299.03
PP-hBNN-1	26.31	37.39	16.25	311.77
PP-hBNN-2	30.76	-	9.75	382.05
PP-hBNN-3	39.49	-	7.78	591.25
PP-hBNN-5	34.97	-	5.62	666.41

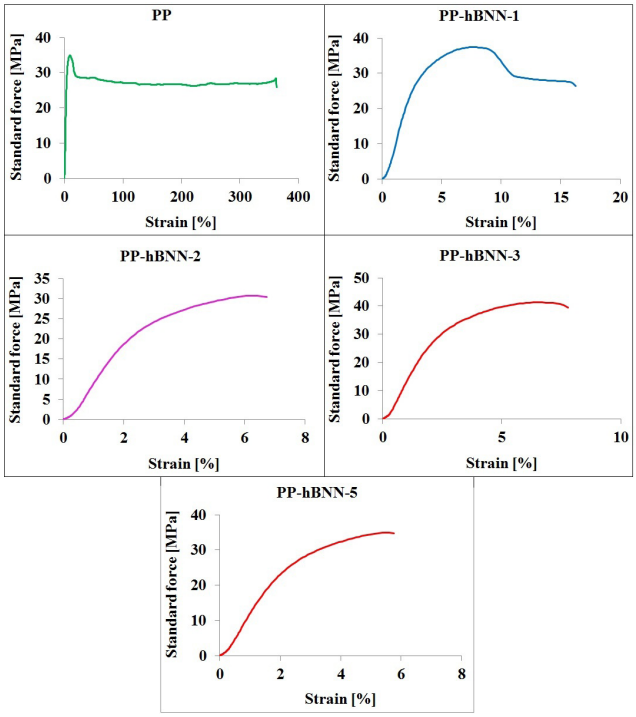

Fig. 7 Stress-strain curves of the neat ***PP*** and PP-h-BNN nanocomposite films

It was observed that as the filling ratio of the prepared films increased, the rigidity of the nanocomposites gets stronger than neat PP. When compared with neat PP with 3 wt% h-BNN content, the tensile strength, and elastic modulus of the nanocomposite 39.49 and 591.25 MPa, shows an improvement of 52.7% and 97.7%, respectively. This improvement can be attributed to the high mechanical strength of h-BNNs, uniform dispersion and interaction between h-BNN and the PP matrix. However, there is a slight decrease in tensile strength of the nanocomposite was observed after a critical filling ratio which is 3 wt%. During the stretching process, the arrangement of the PP chains changes due to the applied stress. With the addition of the h-BNN particles, the movement and orientation of the polymer chains are also hindered which causes rigidity and a sharp decrease of the elongation at break. This behavior is a common observation for PP composites reinforced with fillers whether micro- or nano-scale dimensions. In literature, it is reported that with the addition of a small amount of nanoparticles tensile strength, yield strength, and modulus increase. This situation is attributed to the strong interaction between the particle interface and the matrix [32, 33].

As can be seen in Table 3, neat PP shows yield strength, and with the addition of 1 wt% h-BNN yield strength increases. But at other filling ratios nanocomposites don't show any yield. This can be attributed to decreased interaction between h-BNN particles and PP matrix due to the stacking layers of particles which is also proved by the SEM images (Fig. 8).

3.2.3 Morphological features

All properties of the nanocomposites are affected by the dispersion of the nanofiller. Homogeneity is a key factor in improving the properties of the matrix. The dispersion efficiency of the h-BNNs in the PP matrix was evaluated by SEM and STEM analyses.

SEM analyses which were conducted on the fractured surface of the nanocomposite films were shown in Fig. 8(c)–(d) and confirmed that exfoliated h-BNNs are homogeneously dispersed in the PP matrix without agglomeration at lower h-BNN content as 1 wt%. Even though the particle dispersion still seemed homogenous at higher h-BNN contents from Fig. 8(d), weak Van der Waals interactions take place and stacking of the few h-BNN layers occurs ascendant (pointed by circles). Over a content of 3 wt%, the dispersion effect weakens.

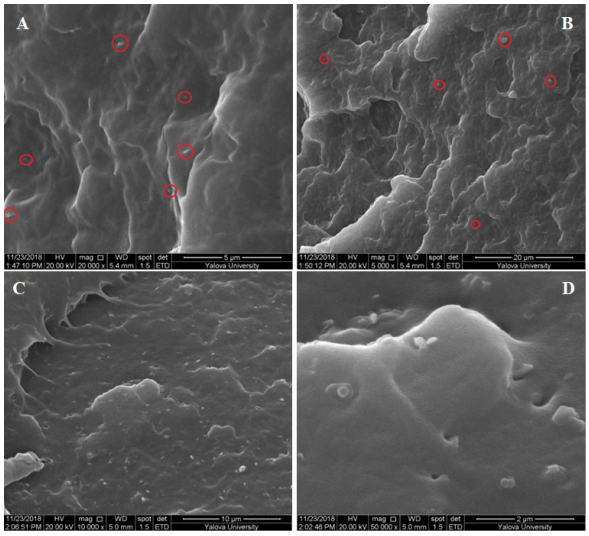

Fig. 8 SEM images of (a) PP-h-BNN nanocomposite films containing 1%wt h-BNN; (b) nanocomposite films containing 2%wt h-BNN; (c) films containing 2%wt h-BNN at 10000X magnification; (d) films containing 2%wt h-BNN at 50000X magnification

3.2.4 Rheological properties

Since all the ingredients are responsible for the properties of the nanocomposite, it is necessary to study the effect of particle content which is used for film production. The frequency dependency of the storage (G′) and loss (G″) moduli of PP-h-BNN nanocomposite films as a function of h-BNN loading at 190 °C are given in Fig. 8. Storage modulus is the ability of the material to store energy and loss modulus is the ability of the material to dissipate energy [34]. It can be clearly seen that the addition of h-BNN significantly enhances the moduli of PP over the entire frequency range. Even though they do not differ in the low-frequency region, G′ and G″ increase simultaneously with increasing h-BNN loading in the high-frequency region. The crossover frequency is a frequency value of a viscoelastic material where it changes its rheological behavior from the rubbery plateau region to the terminal region, and it is determined as the frequency values which intersect the G′ and G″ values [35].

One can see from Fig. 9 that for PP matrix as the frequency increases, both G′ and G″ increase. The pure matrix behaves like an elastic solid since $G' > G''$ at lower frequencies.

As the frequency increases, the G′ increases; it crosses the loss modulus at 72 rad·s^{-1} and this point is called the cross-over point. From the cross-over point, viscous behavior dominates. However, with the addition of h-BNN behavior of the PP matrix changes and all h-BNN-containing samples don't show a cross-over point.

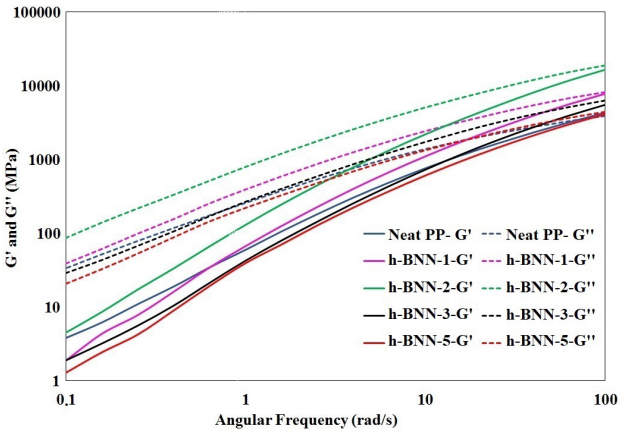

Fig. 9 Variations in G′ and G″ and angular frequency of neat ***PP*** and PP-h-BNN nanocomposite films

It is known that complex viscosity depends on the G′ and indicates the ability of the media to show maximum resistance to flow and deformation [34]. Fig. 10 reveals that with the increment of h-BNN content reveals a decrement in complex viscosity. With the addition of h-BN into the PP matrix, polymer chains surround the particles and cause a high immobile monolayer around them. The non-contact polymer chains become constrained due to the interaction with polymer chains of the immobile monolayer, so, the overall mobility of the nanocomposite decreases. As a result, the complex viscosity decreases with the increasing amount of h-BNN up to 5 wt% However, with the increasing amount of h-BNN content stacking of h-BNN particles starts.

h-BNNs probably get stacked due to the presence of weak and non-local Van Der Waals forces, which causes difficulty in proper dispersion and alignment in the PP matrix. Furthermore, this stacking leads to a slight decrease in the thermal and mechanical properties of the composites after an optimum h-BNN content.

4 Conclusion

FT-IR, XRD and morphological analysis (SEM and STEM) of h-BNNs prove that the exfoliation process was successful. PP-based nanocomposite films reinforced with h-BNNs with different filler content were prepared via the melt extrusion method. Thermal, mechanical, morphological, and rheological properties of the nanocomposite films were investigated. TGA and OIT analysis shows enhancement in the thermal stability of nanocomposites.

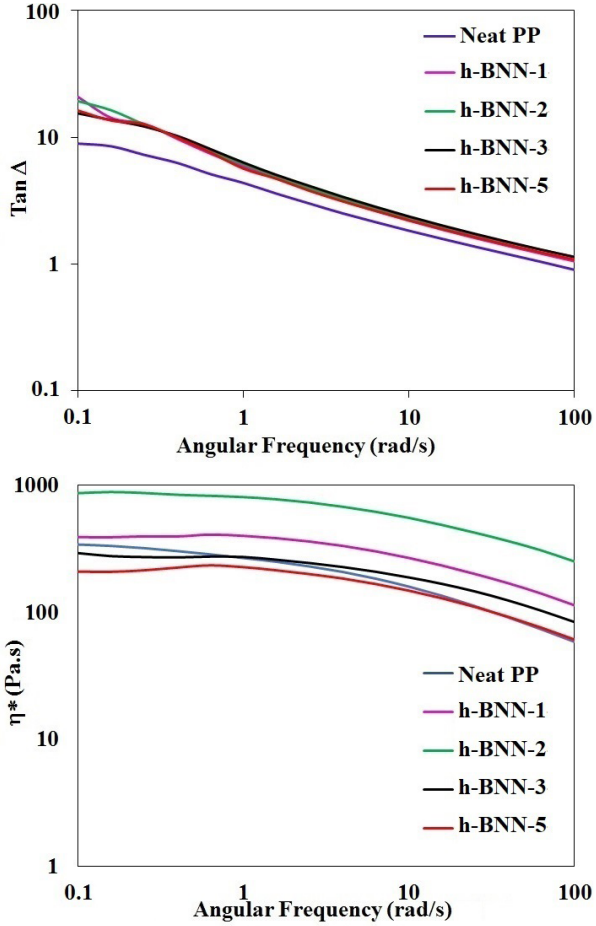

Fig. 10 Rheological properties of nanocomposite films; (a) Tan δ as a function of angular frequency; (b) complex viscosity as a function of the angular frequency of the neat PP and PP-h-BNN nanocomposite films

T_m and T_c increased with the increased the weight fraction of h-BNNs which also proves the increased thermal stability. The rheological analysis showed that the viscosity of the nanocomposites are higher than the neat PP matrix. The storage modulus and loss modulus of polymers elevate with increasing frequency. The prepared nanocomposite films may serve as an alternative protective packaging material, especially in high thermal and mechanical properties are demanded.

Acknowledgments

This study was supported by Yalova University Scientific Research Projects Coordination Department (Project no. 2018/DR/0006). The authors also would like to thank Assoc.Prof. Dr. Alper Kaşgöz for his support of rheological analysis.

References

[1] Liu, Y., Gao, Y., Wang, Q., Lin, W. "The synergistic effect of layered double hydroxides with other flame retardant additives for polymer nanocomposites: a critical review", Dalton Transactions, 47(42), pp. 14827–14840, 2018. https://doi.org/10.1039/C8DT02949K

[2] Adhikari, M., Orasugh, J. T., Chattopadhyay, D. "17 - Biomedical application of polymer-graphene composites", In: Rahaman, M., Nayak, L., Hussein, I. A., Das, N. C. (eds.) Polymer Nanocomposites Containing Graphene: Preparation, Properties, and Applications, Woodhead Publishing, 2022, pp. 507–535. ISBN 978-0-12-821639-2 https://doi.org/10.1016/B978-0-12-821639-2.00011-2

[3] Karak, N. "Chapter 1 - Fundamentals of Nanomaterials and Polymer Nanocomposites", In: Nanomaterials and Polymer Nanocomposites: Raw Materials to Applications, Elsevier, 2019, pp. 1–45. ISBN 978-0-12-814615-6 https://doi.org/10.1016/B978-0-12-814615-6.00001-1

[4] Youssef, A. M. "Polymer Nanocomposites as a New Trend for Packaging Applications", Polymer-Plastics Technology and Engineering, 52(7), pp. 635–660, 2013. https://doi.org/10.1080/03602559.2012.762673

[5] Bayramoğlu, G., Şeker, M. G., Mudu, M. "Preparation of Methacrylated Polyglycidol-POSS Based Silver Nanoparticle Containing Nanocomposites via Photopolymerization", Progress in Organic Coatings, 101, pp. 510–521, 2016. https://doi.org/10.1016/j.porgcoat.2016.09.021

[6] Doagou-Rad, S., Islam, A., Merca, T. D. "An application-oriented roadmap to select polymeric nanocomposites for advanced applications: A review", Polymer Composites, 41(4), pp. 1153–1189, 2020. https://doi.org/10.1002/pc.25461

[7] Simionescu, B., Ursu, C., Cotofana, C., Olaru, M. "Versatility of Silsesquioxane-Based Materials for Antimicrobial Coatings", presented at 1st International Electronic Conference on Materials session Functional Materials and Interfaces for Biomedical Applications, Basel, Switzerland, May, 26 – June, 10, 2014. https://doi.org/10.3390/ecm-1-c001

[8] Gupta, P., Toskha, B. G. "24- Packaging applications of polymer-graphene composites", In: Rahaman, M., Nayak, L., Hussein, I. A., Das, N. C. (eds.) Polymer Nanocomposites Containing Graphene: Preparation, Properties, and Applications, Woodhead Publishing, 2022, pp. 713–743. ISBN 978-0-12-821639-2 https://doi.org/10.1016/B978-0-12-821639-2.00023-9

[9] Jancar, J., Douglas, J. F., Starr, F. W., Kumar, S. K., Cassagnau, P., Lesser, A. J., Sternstein, S. S., Buehler, M. J. "Current issues in research on structure–property relationships in polymer nanocomposites", Polymer, 51(15), pp. 3321–3343, 2010. https://doi.org/10.1016/j.polymer.2010.04.074

[10] Sattar, M. A. "Interface Structure and Dynamics in Polymer-Nanoparticle Hybrids: A Review on Molecular Mechanisms Underlying the Improved Interfaces", Chemistry Select, 6(20), pp. 5068–5096, 2021. https://doi.org/10.1002/slct.202100831

[11] Fu, S., Sun, Z., Huang, P., Li, Y., Hu, N. "Some basic aspects of polymer nanocomposites: A critical review", Nano Materials Science, 1(1), pp. 2–30, 2019. https://doi.org/10.1016/j.nanoms.2019.02.006

[12] Liu, F., Hu, N., Zhang, J., Atobe, S., Weng, S., Ning, H., Liu, Y., Wu, L., Zhao, Y., Mo, F., Fu, S., Xu, C., Alamusi, Yuan, W. "The interfacial mechanical properties of functionalized graphene-polymer nanocomposites", RSC Advances, 6(71), pp. 66658–66664, 2016. https://doi.org/10.1039/C6RA09292F

[13] Ashraf, M. A., Peng, W., Zare, Y., Rhee, K. Y. "Effects of Size and Aggregation/Agglomeration of Nanoparticles on the Interfacial/Interphase Properties and Tensile Strength of Polymer Nanocomposites", Nanoscale Research Letters, 13(1), 214, 2018. https://doi.org/10.1186/s11671-018-2624-0

[14] Arenal, R., Lopez-Bezanilla, A. "Boron nitride materials: An overview from 0D to 3D (nano)structures", WIRES Computational Molecular Science, 5(4), pp. 299–309, 2015. https://doi.org/10.1002/wcms.1219

[15] Ertug B. "Powder Preparation, Properties and Industrial Applications of Hexagonal Boron Nitride", In: Ertuğ, B. (ed.) Sintering Applications, IntechOpen, 2013, pp. 33–55. ISBN 978-953-51-0974-7 https://doi.org/10.5772/53325

[16] Li, Q., Chen, L., Gadinski, M. R., Zhang, S., Zhang, G., Li, H. U., Iagodkine, E., Haque, A., Chen, L., Q., Jackson, T. N., Wang, Q. "Correction: Corrigendum: Flexible high-temperature dielectric materials from polymer nanocomposites", Nature, 536(7614), 112, 2016. https://doi.org/10.1038/nature17673

[17] Weng, Q., Wang, X., Zhi, C., Bando, Y., Golberg, D. "Boron Nitride Porous Microbelts for Hydrogen Storage", ACS Nano, 7(2), pp. 1558–1565, 2013. https://doi.org/10.1021/nn305320v

[18] Gonzalez-Ortiz, D., Salameh, C., Bechelany, M., Miele, P. "Nanostructured boron nitride–based materials: synthesis and applications", Materials Today Advances, 8, 100107, 2020. https://doi.org/10.1016/j.mtadv.2020.100107

[19] Ali, M., Abdala, A. "Large scale synthesis of hexagonal boron nitride nanosheets and their use in thermally conductive polyethylene nanocomposites", International Journal of Energy Research, 46(8), pp. 10143–10156, 2022. https://doi.org/10.1002/er.7149

[20] Jin, C., Lin, F., Suenaga, K., Iijima, S. "Fabrication of a Freestanding Boron Nitride Single Layer and Its Defect Assignments", Physical Review Letters, 102(19), 195505, 2009. https://doi.org/10.1103/PhysRevLett.102.195505

[21] Han, R., Khan, M. H., Angeloski, A., Casillas, G., Yoon, C. W., Sun, X., Huang, Z. "Hexagonal Boron Nitride Nanosheets Grown via Chemical Vapor Deposition for Silver Protection", ACS Applied Nano Materials, 2(5), pp. 2830–2835, 2019. https://doi.org/10.1021/acsanm.9b00298

[22] Joy, J., George, E., Haritha, P., Thomas, S., Anas, S. "An overview of boron nitride based polymer nanocomposites", Journal of Polymer Science, 58(22), pp. 3115–3141, 2020. https://doi.org/10.1002/pol.20200507

[23] Wang, X. B., Weng, Q., Wang, X., Li, X., Zhang, J., Liu, F., Jiang, X. F., Guo, H., Xu, N., Golberg, D., Bando, Y. "Biomass-Directed Synthesis of 20 g High-Quality Boron Nitride Nanosheets for Thermoconductive Polymeric Composites", ACS Nano, 8(9), pp. 9081–9088, 2014. https://doi.org/10.1021/nn502486x

[24] Li, X., Hao, X., Zhao, M., Wu, Y., Yang, J., Tian, Y., Qian, G. "Exfoliation of Hexagonal Boron Nitride by Molten Hydroxides", Advanced Materials, 25(15), pp. 2200–2204, 2013. https://doi.org/10.1002/adma.201204031

[25] Matović, B., Luković, J., Nikolić, M., Babić, B., Stanković, N., Jokić, B., Jelenković, B. "Synthesis and characterization of nanocrystaline hexagonal boron nitride powders: XRD and luminescence properties", Ceramics International, 42(15), pp. 16655–16658, 2016. https://doi.org/10.1016/j.ceramint.2016.07.096

[26] ISO "ISO 527-3:2018 Plastics – Determination of tensile properties – Part 3: Test conditions for films and sheets", International Organization for Standardization, Geneva, Switzerland, 2018. [online] Available at: https://www.iso.org/standard/70307.html [Accessed: 01 November 2018]

[27] ICDD "ICDD 00-34-0421- Boron nitride", International Centre for Diffraction Data, Newtown Square, PA, USA, 2020.

[28] Bafana, A. P., Yan, X., Wei, X., Patel, M., Guo, Z., Wei, S., Wujcik, E. K. "Polypropylene nanocomposites reinforced with low weight percent graphene nanoplatelets", Composites Part B: Engineering, 109, pp. 101–107, 2017. https://doi.org/10.1016/j.compositesb.2016.10.048

[29] Kong, S., Seo, H., Shin, H., Baik, J. H., Oh, J., Kim, Y. O., Lee, J. C. "Improvement in mechanical and thermal properties of polypropylene nanocomposites using an extremely small amount of alkyl chain-grafted hexagonal boron nitride nanosheets", Polymer, 180, 121714, 2019. https://doi.org/10.1016/j.polymer.2019.121714

[30] Zhao, T., Zhang, X. "Enhanced thermal conductivity of PE/BN composites through controlling crystallization behavior of PE matrix", Polymer Composites, 38(12), pp. 2806–2813, 2017. https://doi.org/10.1002/pc.23880

[31] Borysiak, S. "The thermo-oxidative stability and flammability of wood/polypropylene composites", Journal of Thermal Analysis Calorimetry, 119, pp. 1955–1962, 2015. https://doi.org/10.1007/s10973-014-4341-y

[32] Cho, J. W., Paul, D. R. "Nylon 6 nanocomposites by melt compounding", Polymer, 42(3), pp. 1083–1094, 2001. https://doi.org/10.1016/S0032-3861(00)00380-3

[33] Liu, L., Qi, Z., Zhu, X., "Studies on nylon 6/clay nanocomposites by melt-intercalation process", Journal of Applied Polymer Science, 71(7), pp. 1133–1138, 1999. https://doi.org/10.1002/(SICI)1097-4628(19990214)71:7<1133::AID-APP11>3.0.CO;2-N

[34] Sankar, M. R., Jain, V. K., Ramkumar, J., Joshi, Y. M. "Rheological characterization of styrene-butadiene based medium and its finishing performance using rotational abrasive flow finishing process", 51(12), pp. 947–957, 2011. https://doi.org/10.1016/j.ijmachtools.2011.08.012

[35] Kurt, G., Kasgoz, A. "Effects of molecular weight and molecular weight distribution on creep properties of polypropylene homopolymer", Journal of Applied Polymer Science, 138(30), 50722, 2021. https://doi.org/10.1002/app.50722